Analysis of Deformation and Failure of Embankment Slope Under Earthquake

Dengchen Zhou [1, *], Yichang Zhao [2]

[1] School of Earth Sciences, Yunnan University, Kunming, China, 650500

[2] North China University of Water Resources and Electric Power, Zhengzhou, China, 450045

* Corresponding Author Email: zdc13571413337@163.com

Abstract. Earthquakes are among the natural factors that seriously threaten the development of human society and the economy. Earthquakes significantly threaten embankment slope stability, with dynamic responses influenced by seismic wave characteristics, slope geometry, and material properties. This study uses FLAC3D numerical simulation to analyze acceleration, displacement, and stress responses of a mountainous embankment slope under Wolong (WL), Lushan (LS), and Luding (LD) seismic waves. Innovations include the first comparative evaluation of three seismic waves' differential effects, revealing LD waves induced the strongest acceleration amplification (1.5–2 times the slope toe values, 0.1–0.2 s time lag) while LS waves caused the highest stress increments (LS > LD > WL). A validated local damping model (0.157) combined with free-field boundary conditions improved seismic wave propagation simulation accuracy. Significance lies in providing multi-wave design criteria for seismic zones, validating the Mohr-Coulomb model's applicability to soil elastoplastic behavior, and guiding monitoring strategies. Conclusions show seismic wave type dominantly controls responses, with crest stress mutations (−123%) and mid-slope displacement sensitivity (7.5 mm at 0.5 g) indicating instability risks. The model offers a reliable framework for slope seismic design in complex geological settings.

Keywords: Embankment Slope, Seismic Wave, Dynamic Response, Stress Mutation, Numerical Simulation.

1. Introduction

Earthquakes rank among the most severe natural threats to human society and economic development. In seismically active regions, seismic-induced deformation and failure of embankment slopes can severely compromise transportation safety, leading to substantial casualties and property losses. Thus, investigating the deformation and failure mechanisms of embankment slopes under earthquake loading, and optimizing their design and safety maintenance, holds significant societal and practical value.

The dynamic behavior of slopes under seismic excitation has long been a focal point in geotechnical and seismic engineering. Substantial research has been conducted globally, integrating field investigations, physical modeling, and numerical simulations. For instance, Li et al.[1] employed discrete element numerical modeling to analyze the dynamic response of soft-hard interbedded bedding rock slopes. Yang et al.[2] examined the effects of seismic traveling wave and uniform excitations on high rock slope behavior. Liu et al.[3] utilized the UDEC discrete element software to simulate the seismic response of anti-dip soft-hard interbedded rock slopes.

Studies have highlighted that seismic wave propagation characteristics, slope geological configurations, and material properties collectively govern slope dynamic behavior. Seismic wave input parameters—frequency, amplitude, and duration—significantly impact slope stability (Zhang et al.[4]). Soft-hard rock layers amplify seismic acceleration, with soft rock demonstrating more pronounced amplification (Wang et al.[5]). Additionally, seismic wave spectral characteristics manifest as fixed frequency band amplifications during transmission from hard to soft rock (Chen et al.[6]).

Slope instability failure modes represent a critical aspect of seismic stability analysis. Earthquake-induced slope failures primarily occur via sliding and collapse, with modes varying according to

lithology and ground motion characteristics (Liu et al.[3]). For example, Liu et al.[3] identified that fractures in weak layers serve as key tensile failure zones due to repeated seismic wave loading. Yang et al.[2] noted that traveling wave excitation alters seismic wave propagation in slope media or at the slope toe, thereby changing instability failure modes.

To accurately simulate slope dynamic behavior under earthquakes, multi-scale simulation methods are increasingly vital. Integrating macro- and micro-scale approaches enables comprehensive understanding of earthquake-induced deformation and failure processes (Zhao et al.[7]). Li et al.[8] utilized three-dimensional discrete element technology to investigate the dynamic response and instability mechanisms of soft-hard interbedded slopes, offering a valuable framework for multi-scale simulation development.

In summary, the dynamic response and failure mechanisms of embankment slopes under seismic loading are intricate, dependent on seismic wave properties, geotechnical characteristics, and slope geometry. Building on prior research, this study employs FLAC3D numerical modeling to investigate the dynamic behavior and failure mechanisms of embankment slopes under earthquake loading. The findings aim to provide a theoretical foundation for designing and maintaining embankment slopes in high-risk seismic regions.

2. Establishment of numerical model for slope dynamic analysis

2.1. Geometric Dimensions and Monitoring Point Layout

The model is defined in a Cartesian coordinate system with dimensions extending 20 m along the x-axis, 2 m along the y-axis, and 30 m along the z-axis, as illustrated in Fig. 1. During the meshing of the slope dynamic analysis numerical model, strict criteria must be adhered to ensure computational accuracy and reliability.According to Kuhlemeyer, element sizes must be smaller than 1/8–1/10 of the wavelength corresponding to the highest frequency of the input seismic motion(Kuhlemeyer et al.[9]).To investigate the effect of seismic motion amplitude on the dynamic response of the rock slope, the selected slope model and monitoring point layout are presented in Fig. 1. Monitoring points are uniformly distributed along the slope profile at increasing elevations to capture elevation-dependent response characteristics.

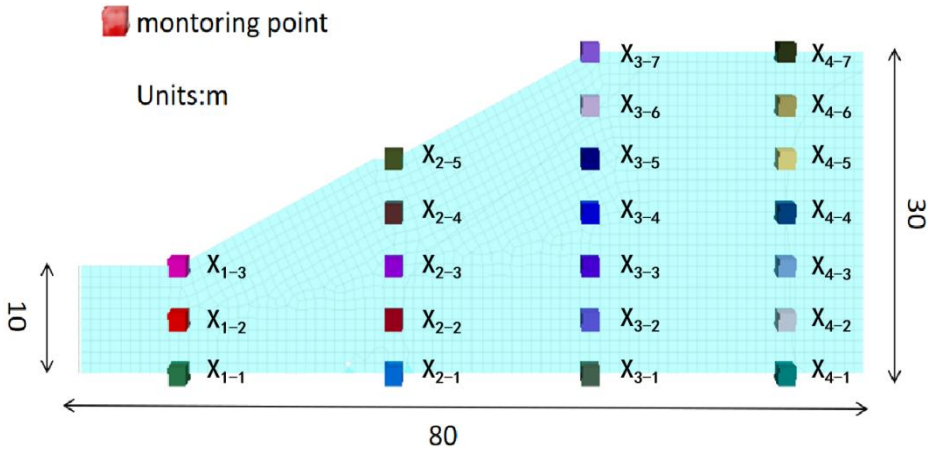

Figure 1. Geometric size of slope model and arrangement of monitoring points

2.2. Mechanical parameters of materials

The material group involved in the model is ' clay ', and its mechanical parameters are shown in Table 1:

Table 1. Material mechanics parameter table

Material Grouping	Density (kg/m^3)	Young's modulus (Pa)	Poisson ratio	Angle of internal friction (°)	Force of cohesion (Pa)
Soil	2000.0	500×10^6	0.3	25	30×10^3

The parameters were established through field geological surveys, indoor geotechnical tests, and consultation of relevant engineering experience and literature. Key material properties are summarized in Table 1.

Density, defined as the mass per unit volume (kg/m³), quantifies the material's compactness. Young's modulus (Pa) represents the material's stiffness, or resistance to elastic deformation under stress. Poisson's ratio, a dimensionless parameter, is the ratio of transverse to longitudinal strain during uniaxial loading. The internal friction angle (°) and cohesion (Pa) collectively characterize the material's shear strength, with the former reflecting frictional resistance and the latter adhesive forces between particles.

2.3. Boundary Conditions

2.3.1. Static Boundaries

During static analysis, boundary conditions are typically set at a sufficient distance from the slope. Given the slope's constraints by surrounding soil/rock in real-world applications, the model remains in stable equilibrium during static analysis. The location and configuration of fixed boundaries influence model stress and deformation results, necessitating determination based on site-specific boundary conditions and engineering expertise.

2.3.2. Dynamic Boundaries

Free field boundaries are employed to simulate wave propagation in unbounded domains. This method couples free field grids to lateral structural boundaries via viscous dampers, ensuring incoming waves are efficiently absorbed and energy reflection is minimized. This configuration more accurately replicates seismic wave propagation and attenuation in natural settings, providing realistic dynamic response predictions for slope boundaries under earthquake loading.

Implementation of free field boundaries requires the base to be horizontal and normals to lateral boundaries to align perpendicularly with the slope surface. When these conditions are met, free field boundaries effectively simulate seismic wave propagation and attenuation, validating their suitability for dynamic slope analysis.

2.4. Initial conditions

2.4.1. Initial state of displacement

The initial displacement of all grid points in the model area is zeroed, and only the influence of dynamic action on the displacement is studied. It shows that there is no displacement in the x, y and z directions of the slope soil at the beginning of the model calculation, and it is kept in a static state. The initial displacement setting before the calculation of this model is due to the assumption that the model is subjected to load. Therefore, the subsequent dynamic analysis is also set according to the initial state.

2.4.2. Initial Velocity State

Initial displacements of all nodes within the model domain are set to zero to isolate the effects of dynamic loading on displacement. This ensures the slope soil remains in static equilibrium with zero displacement in all (x, y, z) axes at the simulation onset. The initialization of zero displacement is premised on the assumption of unloaded initial conditions, providing a basis for subsequent dynamic analyses.

2.5. Loading seismic waves

2.5.1. Acceleration loading method

Acceleration loading is implemented using the command: zone face apply acceleration (1,0,1) table earthquake range position-z -0.1. This applies acceleration within the z-coordinate range of −0.1 m to 0.1 m, with an acceleration vector of (1, 0, 1). This configuration induces 1 g accelerations in the x- and z-directions, while maintaining zero acceleration in the y-direction. To investigate

amplitude effects, acceleration vectors are systematically scaled from (1, 0, 1) to (2, 0, 2) and finally to (5, 0, 5), with time-dependent variations derived from seismic wave datasets.

2.5.2. Waveform feature description

The seismic waves used in this numerical simulation are selected from actual monitoring data in Wenchuan Wolong, Luding, and Lushan. The acceleration time-history curves of these waves are presented in Figs. 2–4.

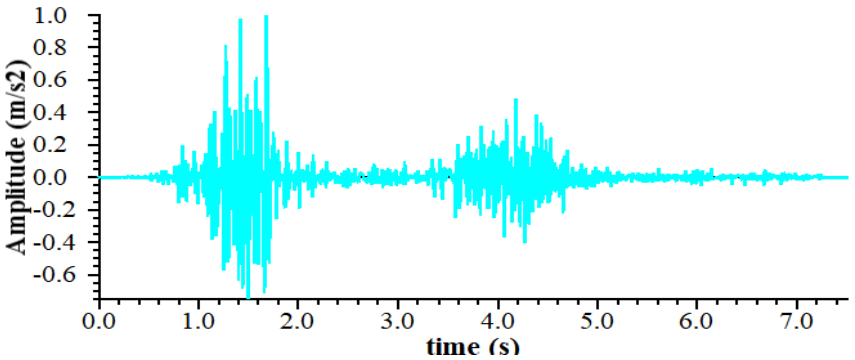

Figure 2. Wolong seismic wave acceleration time history curve

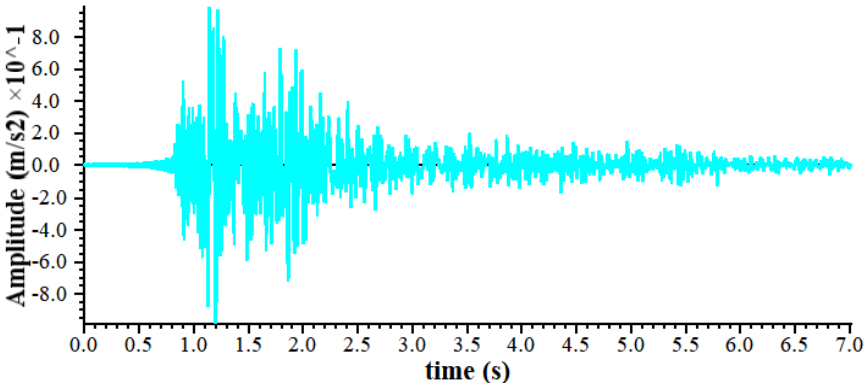

Figure 3. Luding seismic wave acceleration time history curve

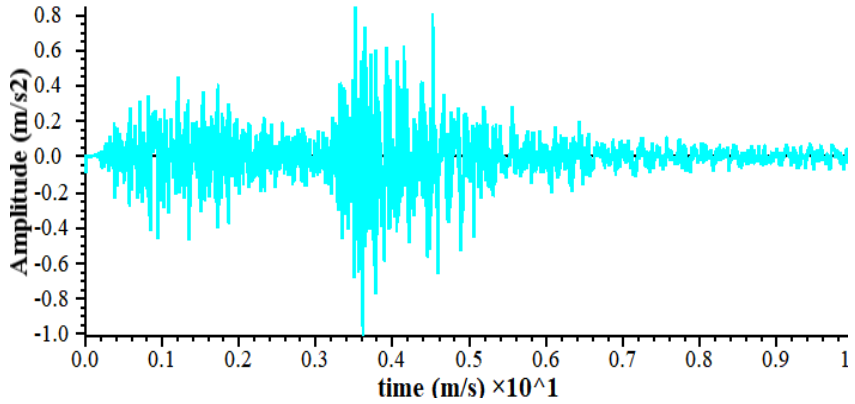

Figure 4. Lushan seismic wave acceleration time history curve

2.6. Damping

The local damping used in this study is of the local damping type. This method exhibits frequency insensitivity, making it well - suited for simple models. Unlike Rayleigh and hysteresis damping, local damping eliminates the need to estimate the model's natural frequency, thereby streamlining computations. Furthermore, its frequency insensitivity permits larger dynamic loading time steps, reducing computational time and enhancing efficiency. The local damping coefficient employed in

this study's slope dynamic analysis model is 0.157, selected based on prior validation against field data.

3. Data Analysis

This section presents results from dynamic response simulations under three seismic waves, focusing on acceleration amplification, displacement distribution, and stress mutations. Key findings include: (1) significant wave-type dependency in acceleration and stress responses; (2) elevation-dependent amplification effects; (3) mid-slope displacement sensitivity; and (4) localized stress concentrations at the crest. These results highlight critical instability mechanisms under seismic loading.

3.1. Analysis of acceleration response characteristics

3.1.1. Comparison of different seismic waves

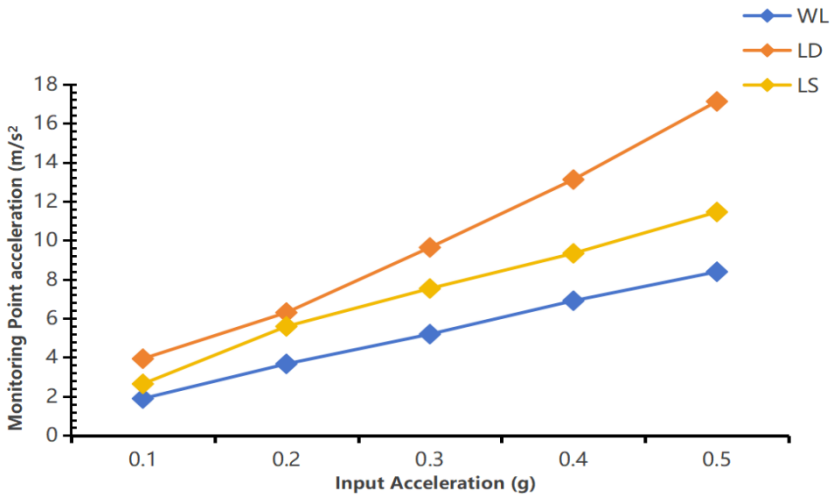

Figure 5. Shows acceleration responses at AX3-7 under WL, LD, and LS waves.

Fig. 5 shows the acceleration response comparative analysis curve of the monitoring point AX3-7 under the action of WL, LD and LS seismic waves, in which the abscissa is the input acceleration and the ordinate is the acceleration of the monitoring point. It can be seen from Fig.5 that under different input acceleration levels, the acceleration values of the monitoring points under the action of three kinds of seismic waves show a linear increasing trend, and the increase rate of the acceleration of the monitoring points of the three kinds of seismic waves is LD > LS > WL. This shows that the acceleration increase of monitoring points caused by different seismic waves is different, and the acceleration response corresponding to LD seismic wave is the most obvious. The type of seismic wave is one of the important factors affecting the dynamic response of structural acceleration.

3.1.2. Comparison of different monitoring points

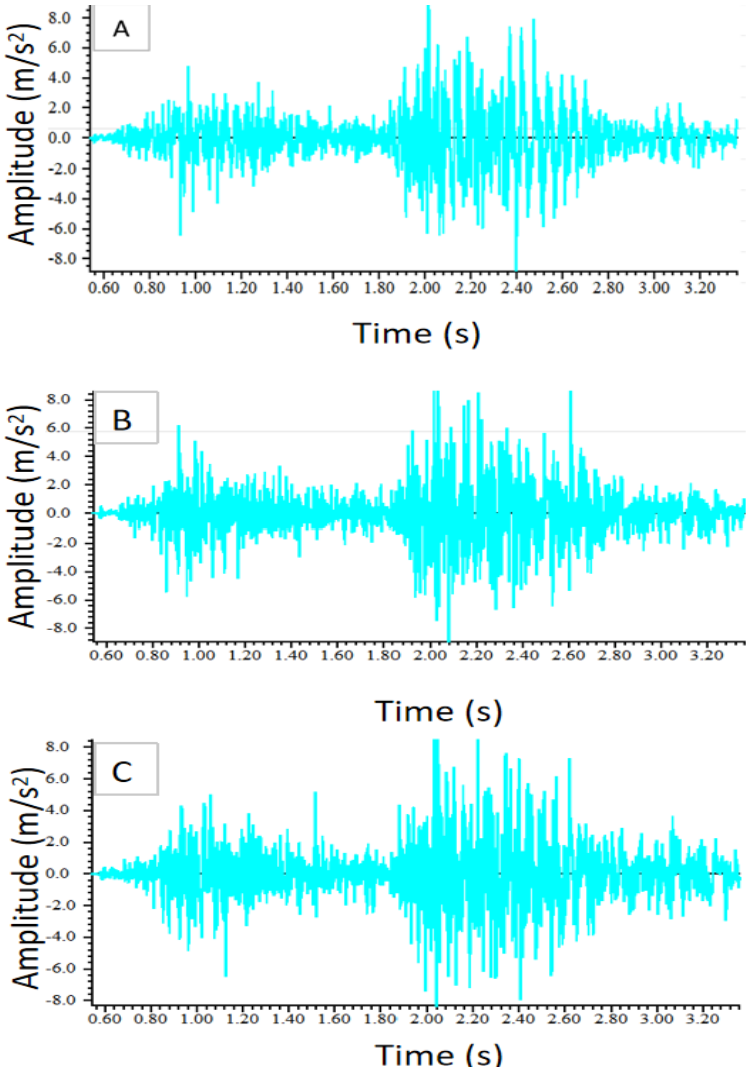

Figure 6. Shows acceleration histories at AX1-3, AX2-5, and AX3-7 under 0.5g LS excitation.

From the monitoring results of Figure 6, it can be seen that under the condition of 0.5g force of LS seismic wave, the acceleration response of the slope along the elevation direction is as follows : the shape of the acceleration time history curve of each monitoring point is basically the same, indicating that the slope has a holistic synergistic deformation under the action of seismic load, and there is no local buckling. The peak acceleration of each point increases significantly with the elevation of the monitoring point, and the results are in line with the prediction of the topographic amplification effect theory. In addition, from the calculation of the phase difference, it can be seen that the propagation of seismic waves from the slope toe of the slope to the top of the slope has a time lag (0.1-0.2s). The main reason is the path change and velocity attenuation of seismic waves propagating in heterogeneous media. The results of this paper can provide reference information for seismic response research and seismic design of high and steep slopes.

3.2. Analysis of displacement response characteristics

3.2.1. Comparison of different monitoring points

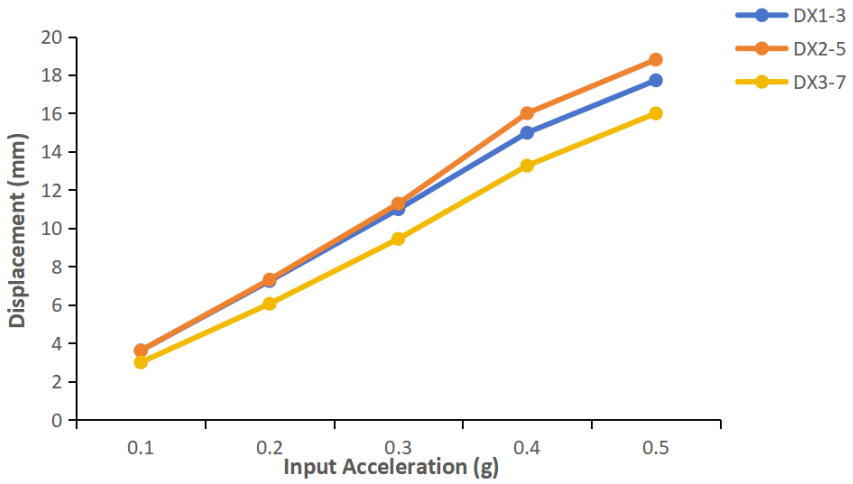

Figure 7. Shows displacement histories at DX1-3, DX2-5, and DX3-7 under LD.

Fig. 7 illustrates displacement histories for three vertically aligned points (DX1-3, DX2-5, DX3-7) under LD seismic waves. Displacements at all points increase with acceleration (0.1–0.5 g), with mid-slope DX2-5 showing the largest amplitudes. At identical accelerations, DX2-5 displacements exceed both lower DX1-3 and higher DX3-7, indicating elevation-dependent sensitivity. This highlights site-specific dynamic responses critical for seismic design.

3.2.2. Input acceleration amplitude influence analysis

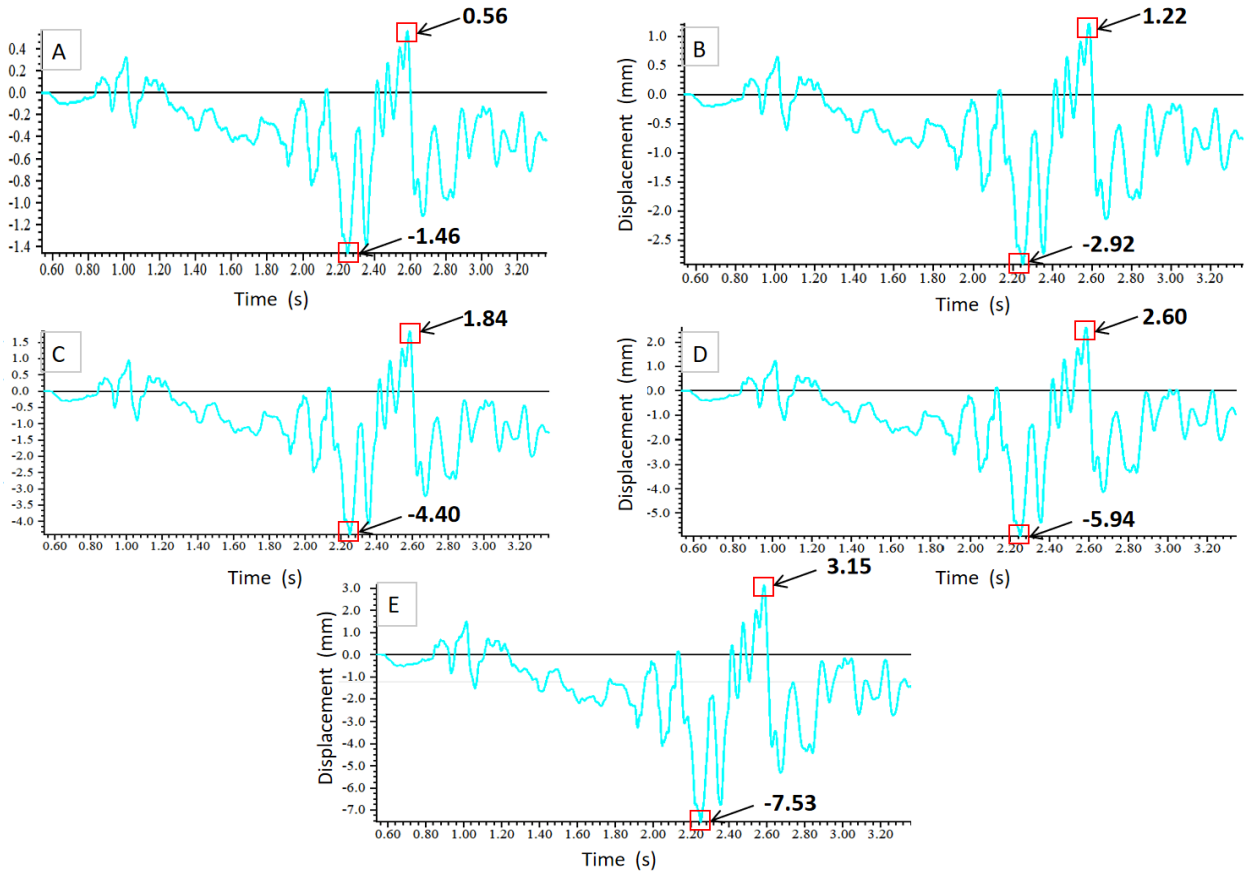

Figure 8. Shows crest displacement at DX3-7 under LS waves with 0.1–0.5 g accelerations (A–E: 0.1 g to 0.5 g).

Fig. 8 shows crest displacement at DX3-7 under LS waves with 0.1–0.5 g accelerations. Displacement amplitudes increase nonlinearly with input intensity: 0.56 mm/−1.46 mm at 0.1 g, 1.84 mm/−4.40 mm at 0.3 g, and 3.15 mm/−7.53 mm at 0.5 g. A critical transition occurs at 0.4 g, where displacements peak at 2.60 mm/−5.94 mm with curve deviation, indicating plastic deformation. These results highlight that high-intensity LS waves significantly elevate dynamic instability risks, providing critical data for slope seismic design.

3.3. Analysis of stress response characteristics

3.3.1. Seismic waves type influence analysis

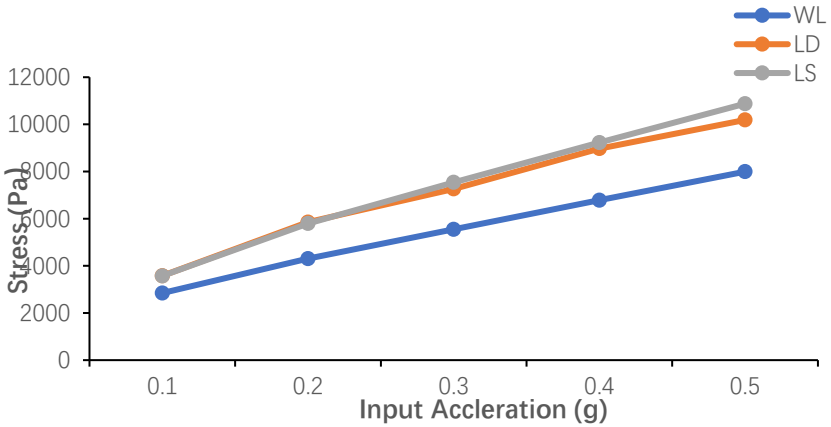

Figure 9. Broken line diagram of stress change of SX4-7 monitoring point on the top of slope under different seismic waves.

Under the action of WL, LD and LS seismic waves, the stress change curve of SX4-7 monitoring point at the top of the slope with the input acceleration is shown in figure 9. The stress corresponding to the three seismic waves increases with the input acceleration from 0.1g to 0.5g. The magnitude of the stress increment is LS seismic wave > LD seismic wave > WL seismic wave ; it can be seen that the seismic wave type will have different degrees of influence on the stress response of the slope top, and the dynamic stress effect caused by the LS seismic wave is the largest, which provides the necessary data for the seismic design of different seismic wave response dynamic effects in the project.

3.3.2. Analysis of slope elevation effect

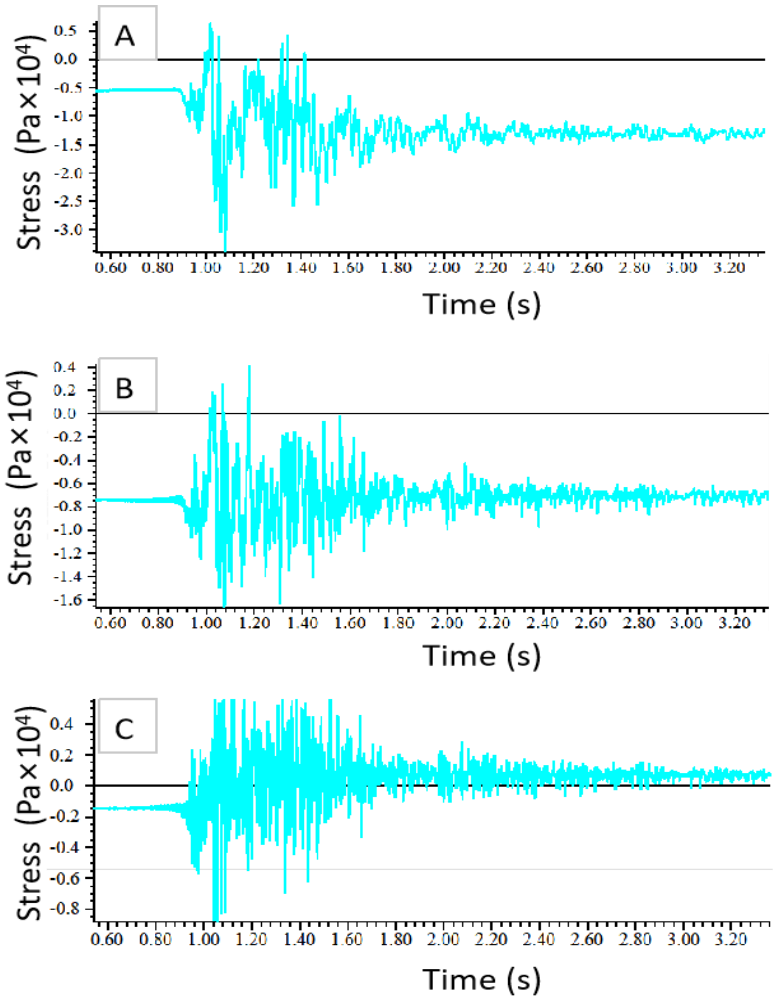

Figure 10. Shows stress histories at DX2-5, DX3-7, and DX4-7 under 0.5 g LD.

Fig. 10 shows mid-slope DX2-5 exhibits the strongest tensile stress response, peaking at 8.0 kPa before dropping abruptly to −2.0 kPa at t=1.6 s. Mid-slope DX3-7's peak stress lags DX2-5 by 0.2 s, reflecting wave transmission delays. Crest DX4-7 shows minor stress variation (−1.5 kPa to 6.5 kPa) but sudden stress mutations (−123% at t=1.4 s), indicating heightened crest sensitivity to dynamic loading.

4. Result

This study systematically investigates the dynamic response characteristics and failure mechanisms of embankment slopes under earthquake loading using FLAC3D numerical modeling. Key findings include: (1) Seismic wave type significantly governs dynamic response, with Luding (LD) waves inducing the largest acceleration amplification (LD > LS > WL) and Lushan (LS) waves exerting the strongest dynamic stress effects (LS > LD > WL); (2) Acceleration responses exhibit a pronounced elevation amplification effect, with crest peak accelerations 1.5–2 times greater than slope toe values and a 0.1–0.2 s propagation delay, attributed to wave velocity attenuation in heterogeneous media; (3) Displacement responses demonstrate spatial differentiation, with mid-slope points (e.g., DX2-5) most sensitive to LD-induced displacement, reaching 7.5 mm at 0.5 g and showing plastic deformation at 0.4 g; (4) The slope is susceptible to stress discontinuities (up to −123% stress change at the crest) and dynamic instability under high-intensity earthquakes, particularly under LS waves; (5) Model validation confirms free field boundaries, local damping (0.157), and the Mohr-Coulomb constitutive model effectively simulate wave propagation and soil elastoplastic behavior,

aligning with theoretical predictions. These results provide critical insights for seismic design and stability analysis of high-steep slopes in seismically active regions.

5. Conclusion

This study systematically investigates the dynamic response and failure mechanisms of embankment slopes under seismic loading using FLAC3D numerical modeling. Key findings highlight the critical role of seismic wave type, elevation effects, and material properties in governing slope behavior. The Luding wave induces the most significant acceleration amplification ((1.5–2 times the slope toe values, 0.1–0.2 s time lag), while the Lushan wave causes the highest stress increments. Mid-slope regions exhibit the largest displacements (up to 7.5 mm at 0.5 g), and crest stress mutations (−123%) indicate localized instability risks. Model validation confirms the effectiveness of free-field boundaries and the Mohr-Coulomb constitutive model in simulating wave propagation and soil elastoplasticity.

5.1. Practical Applications

The results provide a framework for seismic design of embankment slopes in high-risk regions, guiding the selection of appropriate wave input parameters and monitoring strategies. The elevation-gradient monitoring method can be applied to identify critical stress concentration zones, while the validated numerical model offers cost-effective alternatives to physical testing for engineering optimization.

5.2. Future Directions

Future research should focus on: (1) integrating long-term cyclic loading effects to evaluate cumulative damage; (2) extending the model to include groundwater-seismic coupling; (3) validating results through full-scale field tests; (4) developing hybrid models that combine macro-scale FLAC3D with micro-scale discrete element simulations to capture complex failure processes in heterogeneous slopes. These advancements will enhance the resilience of embankment infrastructure in seismically active areas.

References

[1] Li, S. Y., Wu, Q., Wang, L. Q., & et al. (2023). Dynamic response of soft-hard interbedded bedding rock slopes under earthquake action. Earth Science, 48 (8), 3127 – 3136.

[2] Yang, Q., Chen, Z. L., Li, G. F., & et al. (2024). Dynamic response analysis of high rock slopes under traveling wave and uniform excitations. Water Resources and Hydropower Engineering, 55 (9), 164 – 177.

[3] Liu, Y. P., Deng, H., Huang, R. Q., & et al. (2012). Numerical simulation of seismic response of anti-dip soft-hard interbedded rock slopes. Hydrogeology & Engineering Geology, 39 (3), 30 – 37.

[4] Qi, S. W., Wu, F. Q., & Sun, J. Z. (2003). Study on dynamic response laws of slopes. Science in China Series E: Technological Sciences, 33 (S1), 28 – 40.

[5] Li, L. Q., Zhang, S., He, C., & et al. (2020). Dynamic response and instability mechanism of soft-hard interbedded slopes based on discrete element technology. Water Resources and Hydropower Engineering, 51 (4), 203 – 211.

[6] Dong, J. Y., Yang, G. X., Wu, F. Q., & et al. (2011). Large-scale shaking table test on dynamic response and failure mode of bedding rock slopes under earthquake. Rock and Soil Mechanics, 32 (10), 2977 – 2983.

[7] Li, X. L., Tang, H. M., & Wang, L. C. (2014). Centrifuge test on seismic dynamic failure of bedding rock slopes. Chinese Journal of Rock Mechanics and Engineering, 33 (4), 729 – 736.

[8] Cao, Y. B., Dai, F. C., Xu, C., & et al. (2011). Discrete element simulation of deformation and movement mechanism of Tangjiashan landslide. Chinese Journal of Rock Mechanics and Engineering, 30 (S1), 2878 – 2887.

[9] Kuhlemeyer, R. L., & Lysmer, J. (1973). Finite element method for seismic response analysis of earth slopes. Bulletin of the Seismological Society of America, 63 (4), 1169 – 1189.

[10] Hu, X. W., Huang, R. Q., Shi, Y. B., & et al. (2009). Analysis of river-blocking mechanism of Tangjiashan landslide and dam-break mode of barrier lake. Chinese Journal of Rock Mechanics and Engineering, 28 (1), 181 – 189.

[11] Ren, G. M., Xia, M., Li, G., & et al. (2009). Study on toppling deformation and failure characteristics of steep bedding rock slopes. Chinese Journal of Rock Mechanics and Engineering, 28 (S1), 3193 – 3200.

[12] Ai, C., Feng, C., Li, S. H., & et al. (2010). Experimental study on dynamic response of bedding rock slopes under earthquake. Chinese Journal of Rock Mechanics and Engineering, 29 (9), 1825 – 1832.

[13] Jia, J., Huang, R. Q., Ju, N. P., & et al. (2010). Study on instability mechanism of steep bedding rock slopes under strong earthquakes. Journal of Engineering Geology, 18 (S1), 475 – 481.

[14] Luo, G., Hu, X. W., & Gu, C. Z. (2013). Dynamic instability mechanism and initiation velocity of bedding rock slopes under strong earthquakes. Rock and Soil Mechanics, 34 (2), 483 – 490.

[15] Huang, R. Q. (2009). Mechanism and geomechanically model of landslides triggered by the Wenchuan Ms 8.0 earthquake. Chinese Journal of Rock Mechanics and Engineering, 28 (6), 1239 – 1249.

[16] Huang, R. Q., Li, G., & Ju, N. P. (2013). Shaking table test on dynamic response of stratified rock slopes under strong earthquakes. Chinese Journal of Rock Mechanics and Engineering, 32 (5), 865 – 875.

[17] Wu, F. Q., & Qi, S. W. (2014). Statistical rock mechanics study on mechanical effects of rock mass structure. Journal of Engineering Geology, 22 (4), 601 – 609.